Controlling Internal Organization of Multilayer Poly(methacrylic acid) Hydrogels with Polymer Molecular Weight

Veronika Kozlovskaya[§], Oleksandra Zavgorodnya[§], John F. Ankner,[#]* and Eugenia Kharlampieva[§,&]*

[§]Department of Chemistry, [&]Center for Nanoscale Materials and Biointegration, University of Alabama at Birmingham, Birmingham, AL 35294, USA

[#]Oak Ridge National Laboratory, Spallation Neutron Source, Oak Ridge, TN 37831

(*Correspondence to be addressed: ekharlam@uab.edu and anknerjf@ornl.gov)

Abstract

We report on tailoring the internal architecture of multilayer-derived poly(methacrylic acid) hydrogels by controlling the molecular weight of poly(N-vinylpyrrolidone) PVPON in hydrogen-bonded (PMAA/PVPON) layer-by-layer precursor films. The hydrogels are produced by crosslinking PMAA in the spin-assisted multilayers followed by PVPON release. We found that the thickness, morphology, and architecture of hydrogen-bonded films and the corresponding hydrogels are significantly affected by PVPON chain length. For all systems, an increase in PVPON molecular weight from M_w = 2.5 kDa to 1300 kDa resulted in increased total film thickness. We also show that increasing polymer M_w smooths the hydrogen-bonded film surfaces but roughens those of the hydrogels. Using deuterated *d*PMAA marker layers in neutron reflectometry measurements, we found that hydrogen-bonded films reveal a high degree of stratification which is preserved in the cross-linked films. We observed *d*PMAA to be distributed more widely in the hydrogen -bonded films prepared with small M_w PVPON due to the greater

mobility of short-chain PVPON. These variations in the distribution of PMAA are erased after crosslinking, resulting in a distribution of *d*PMAA over about two bilayers for all M_w but being more largely in the films templated with higher M_w PVPON. Our results yield new insights into controlling the organization of nanostructured polymer networks using polymer molecular weight and open opportunities for fabrication of thin films with well-organized architecture and controllable function.

For Table of Contents Use Only

Controlling Internal Organization of Multilayer Poly(methacrylic acid) Hydrogels with Polymer Molecular Weight

Veronika Kozlovskaya, Oleksandra Zavgorodnya, John F. Ankner, and Eugenia Kharlampieva

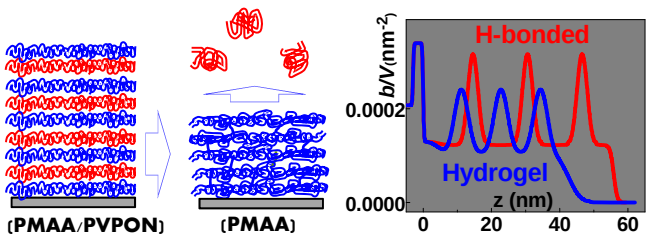

Introduction

Stimuli-sensitive hydrogels afford the capability for drastic and reversible changes in volume under external stimuli, a feature critical in sensing, drug delivery, and tissue engineering applications.[1-12] Among traditional hydrogel parameters, such as crosslink density, composition, and physical dimension,[1,2,3] network architecture has been recently found to greatly influence the behavior of 'bulk' hydrogels.[13-17] On macro- and microscales, a new generation of hydrogels with complex multilayer organization has broken through traditional homogeneously structured networks to be applied in drug delivery, tissue regeneration, and medical devices.[18-21] Hydrogel architecture has proven crucial for regulating hydration and mechanical properties of cellulose-based macrogels.[18] Controlling microstructures of 3D sol-gel transitional hydrogels has been found essential for modulating cell behaviors.[19] A multilayer organization of hyaluronic acid-based hydrogel simulated native 3D cell matrices has been developed for co-culturing several cancer cell lines.[20]

Recently, thin layer-by-layer (LbL)-derived networks have aroused considerable interest as they offer thickness, crosslink density, and swelling/shrinkage variation regulated with a nanoscale precision.[22-27,28] One way of producing these hydrogels is by the covalent crosslinking of LbL coatings as a post-assembly step. Importantly, these networks are not limited to a specific substrate shape, size, or morphology and can undergo fast and dramatic volume changes in response to stimuli.[29-39] Regardless of their nanoscale thickness, these hydrogels can accommodate a large load of biological and synthetic molecules including proteins, peptides, enzymes, and drugs.[11,40,41,42,43] Despite their intriguing properties, there has been little control over the internal structure of these networks that considerably limits the rational design of structured films of complex architecture and composition. LbL-derived hydrogels have been explored by controlling assembly routes,

chemical composition, and thickness, rather than internal organization.[22,36,39] The major challenge in the fabrication of thin hydrogel coatings with controlled structural organization is regulating assembly and crosslinking conditions to control chain entanglements and intermixing. Another difficulty arises from the limited suite of instrumental tools capable of determining network architecture at nanometer spatial resolution.

In this respect, neutron reflectivity (NR) offers a unique capability to resolve the internal organization of thin multilayers by probing their interfacial properties using non-labeled (non-deuterated) and labeled (deuterated) polymers. [44-51] In this way, layer organization has been evaluated based on the superlattice modulation induced in the NR profiles by selectively deuterated multilayer component.[40,52,53] The internal layering in hydrogen (H)-bonded and ionically-paired multilayers is mainly controlled by inter- and intra- chain interactions that have been shown to depend on polymer type, deposition conditions, film thickness, and charge balance.[54-57] However, the effect of polymer molecular weight on film organization has been much less investigated and limited to electrostatically assembled multilayers.[58,59,60] Char and coworkers reported that (poly(ethylene imine) (PEI)/PMAA) films with longer PMAA had higher pH-stability by maintaining their well-ordered structure before complete disintegration at low pH.[59] Sukhishvili and collaborators found that quaternized poly(2-(dimethylamino) ethyl methacrylate assembled with low molecular weight PMAA exhibited strong chain intermixing in response to salt annealing.[60] Yet, polymer molecular weight (M_w) can be a powerful parameter to control assembly and post-assembly responses not only in ionically-paired but also in H-bonded multilayers.[61,62,63] Therefore, understanding the effect of molecular weight on the compositional and structural characteristics of LbL films and LbL-derived materials is highly relevant for both fundamental research and practical applications.

In our previous work, we showed that the internal structure of H-bonded poly(methacrylic acid)/ poly(N-vinylpyrrolidone) (PMAA/PVPON) multilayers dictated the architecture of the (PMAA) hydrogel that resulted from chemical crosslinking of the H-bonded films.[40] We found that PMAA hydrogels derived from spin-assisted H-bonded films had a better internal organization than their highly intermixed counterparts produced by conventional dipping.

In the current study, we tune the architecture of PMAA hydrogel films by controlling PVPON molecular weight in the H-bonded (PMAA/PVPON) multilayer precursors. We explore how PVPON M_w affects the internal structure of (PMAA/PVPON) multilayers with selectively deuterated layers, as well as the corresponding (PMAA) hydrogels upon PVPON release. The degree of interlayer diffusion in both types of films is probed by utilizing NR. We are motivated by the fact that thin hydrogels have shown considerable promise in advanced drug release, biomolecular adhesion, ink-jet printing, and gas permeability; [23,37,39,42,43,64,] making control over network structural organization at the nanoscale highly desirable. Complementary to structure, our study uncovers the role of PVPON on the thickness and morphology of the H-bonded films before and after crosslinking. Our work establishes a basis for regulating the assembly of H-bonded multilayers using molecular weight and provides an understanding of the mechanism of LbL-derived network~~s~~ formation, crucial for developing novel responsive materials.

Experimental

Materials

Poly(methacrylic acid) (PMAA, average M_w 100,000 Da), poly(N-vinylpyrrolidone) (PVPON, average M_w 2500 Da (PVPON-2.5), 55000 Da (PVPON-55), 360000 Da (PVPON-360), and 1300000 Da (PVPON-1300)) were purchased from Aldrich. Ethylenediamine (99%+, EDA) was obtained from Fisher Scientific. Deuterated PMAA (*d*PMAA, M_w 198000 Da, PDI=1.1) was purchased from Polymer Source Inc (Canada). 3-(3-Dimethylaminopropyl)-1-ethylcarbodiimide

hydrochloride (99%+, EDC) was purchased from Chem-Impex International. Poly(glycidylmethacrylate) (PGMA) was synthesized from glycidyl methacrylate by radical polymerization with AIBN in 2-butanone as described elsewhere.[65] Ultrapure de-ionized (DI) water with the resistivity of 0.055 μS/cm (18.2 MΩ cm) was used in all experiments (Evoqua). All other chemicals were purchased from Fisher Scientific and used without further purification. Two-inch diameter silicon wafers with one side polished were purchased from the Institute of Electronic Materials Technology (EL-Cat Inc). To control pH and ionic strength, 0.1 M HCl, 0.1 M NaOH, and NaH_2PO_4 (Aldrich) were utilized as received.

Multilayer film construction

Polymers were dissolved in DI water and deposited from 1 mg mL^{-1} aqueous polymer solutions using a spin-assisted LbL technique (Laurell Technologies). Prior to H-bonded multilayer deposition, the silicon wafers were cleaned as described previously and primed with PGMA whose adsorption at pH = 4 from 0.01 M phosphate buffer solution for 15 min yielded a monolayer of 2 nm dry thickness.[66] The layer of PGMA was spin-cast from a 0.1 mg mL^{-1} chloroform solution onto the surface of the Si wafer, followed by heating at 110 °C for 1 hour and rinsing with chloroform. A PMAA layer was then adsorbed on the PGMA-primed wafers from a 1 mg mL^{-1} methanol solution and crosslinked at 100 °C for 40 min, followed by rinsing with DI water. $(PMAA/PVPON)_n$ LbL films were deposited on the precursor-coated wafers as described previously.[40] Briefly, 3 mL shots of PMAA or PVPON solutions in 0.01 M phosphate buffer at pH = 2.5 were sequentially dropped onto clean silicon substrates and rotated for 30 s at 3000 rpm on a spin-coater; then rinsed twice for 30 s with the buffer solution before the deposition of the next layer. Deuterated *d*PMAA was deposited with every fifth or seventh bilayer to provide neutron contrast. The samples were dried with dry nitrogen and brought to Oak Ridge National Lab (ORNL) for neutron reflectivity measurements.

To produce the hydrogels, PMAA layers within the H-bonded multilayers were chemically crosslinked as described previously.[40] Briefly, the films were exposed to EDC solution (5 mg mL^{-1} at pH = 5.0 (0.01 M phosphate buffer) for 40 min, followed by crosslinking with EDA (5 mg mL^{-1}, 0.01 M phosphate buffer, pH = 5.8) for 16 hours. After that, the crosslinked PMAA hydrogel films were submerged into buffer solutions at pH = 8.0 (0.01 M phosphate buffer) for 24 hours, followed by de-swelling of the films in 0.01 M phosphate buffer at pH = 5 (15 min) and drying at ambient conditions.

Ellipsometry

Film thickness measurements were performed using an M2000U spectroscopic ellipsometer (J.A. Woollam) on thin Si wafers (University Wafers). Prior to use, the substrates were thoroughly rinsed with DI water, dried under a stream of filtered nitrogen and used immediately thereafter. For dry films, measurements were performed between 400 nm and 1000 nm at 65°, 70°, and 75° angles of incidence. For data interpretation, the ellipsometric angles, Ψ and Δ, were fitted using a multilayer model composed of silicon, silicon oxide, and the multilayer film to obtain the thickness of the films. The thickness of SiO_2 was measured for each wafer and was determined using known optical constants. The thickness of the multilayer film was obtained by fitting the data using the Cauchy approximation.[30,39,40] Studies of film swelling were performed using a 5 mL liquid flow-through cell (Woollam). The cell was filled with 0.01 M phosphate buffer solution at various pH values and measurements were taken at 70° after 20 minutes of equilibration. The thickness of the multilayer film at each pH was obtained by fitting data, varying A_n, B_n, and C_n. The mean squared error for data fitting was less than 30.

AFM

AFM height images of (PVPON/PMAA) and (PMAA) films were collected on dry samples using a Multimode 8 (Bruker) in the Soft Tapping mode in air. AFM probes were purchased from Bruker

(resonance frequency ~300 kHz, tip radii 10 nm). AFM height images of 1 μm^2 areas were analyzed for micro-roughness using Nanoscope software (Bruker).

Neutron reflectivity

Neutron reflectivity measurements were performed at the Spallation Neutron Source Liquids Reflectometer (SNS-LR) at the ORNL. The reflectivity data were collected using a sequence of 3.25-Å-wide continuous wavelength bands (selected from 2.63 Å < λ < 16.63 Å) and incident angles (ranging over 0.60° < θ < 2.71°). The momentum transfer, $Q = (4\pi \sin \theta/\lambda)$, was varied over a range of 0.008 $Å^{-1} < Q < 0.22$ $Å^{-1}$. Reflectivity curves were assembled by combining seven different wavelength and angle data sets together, maintaining a constant sample footprint and relative instrumental resolution of $\delta Q/Q = 0.03$ by varying the incident-beam apertures. For data analysis, a model previously used in studies of H-bonded multilayers was applied.[40] The fitting parameters are presented in Tables S1-S9 in Supporting Information. The starting values of the thicknesses of portions of the film were taken from ellipsometry measurements and then adjusted to fit the reflectivity curves. The neutron scattering density (related to refractive index) is defined as $\Sigma = b/V$, where b is the monomer scattering length (the sum of the scattering lengths of the constituent atomic nuclei) and V is the monomer volume. Because the scattering contrast between protonated PMAA and PVPON is insignificant, we used an average Σ_h for the protonated PMAA/PVPON bilayers. Layer intermixing was simulated by error function density profiles (Gaussian roughness).[40] In these models, the interfacial width is parameterized as full-width-at-half-maximum, which equals 2.35×σ, the Gaussian width parameter. The average bilayer spacing d_0 and other structural parameters are qualitatively revealed by superlattice and Kiessig-fringe peak spacings. Goodness of fit was determined by minimizing χ^2, constrained to physically reasonable values of thickness and refractive index and consistency with other measurements, such as ellipsometry. Mass balance between pre- and post-cross-linked films was enforced by preserving

the total amount of deuterated material in the models. Practically, this constraint couples scattering density to layer thickness, the quantity $M = (\Sigma_d - \Sigma_h)d$ being preserved, where Σ_d and Σ_h are, respectively, the scattering densities of deuterated marker layer and protonated matrix, and d the thickness of a pure deuterated marker layer. For *d*PMAA, $\Sigma_d = 5.47\times10^{-4}$ and $\Sigma_h = 1.05\times10^{-4}$ nm^{-2}.

Results and Discussions

Fabrication of (PMAA) hydrogel films is schematically illustrated in Figure 1. H-bonded $(PMAA/PVPON)_n$ multilayers (n denotes bilayer number) were deposited by spin-assisted LbL at pH = 2.5 (Fig.1a). The H-bonded films were treated with EDC and EDA solutions at pH = 5, and pH = 5.8, respectively, to selectively crosslink PMAA layers, followed by PVPON release at pH = 8, the procedure established earlier.[30,38,40] Since PVPON acts as a sacrificial binder not involved in chemical crosslinking, it is important to identify its influence on the structure and morphology of both as-cast H-bonded films and in the corresponding crosslinked PMAA networks. To explore the effect of PVPON molecular weight on multilayer assembly and internal organization before and after crosslinking, PVPON of 2.5 kDa, 55 kDa, 360 kDa, and 1300 kDa were used and denoted as PVPON-2.5, PVPON-55, PVPON-360, and PVPON-1300, respectively; while M_w of PMAA was fixed at 100 kDa.

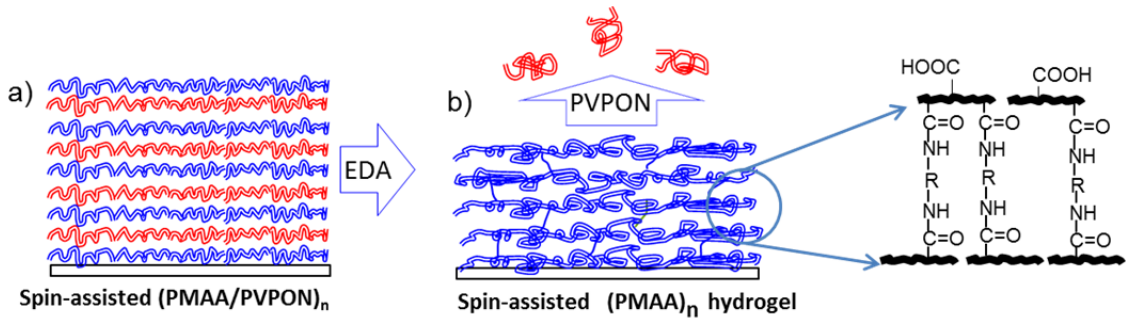

Figure 1. LbL assembly approach for the construction of thin multilayer hydrogels. The initial LbL films are assembled via H-bonded deposition of polymers (a). PMAA layers are crosslinked post-assembly (b). The uncrosslinked PVPON is released from the swollen multilayer hydrogel.

H-bonded film build-up: Effect of PVPON molecular weight

As found with ellipsometry, all H-bonded multilayers grow linearly, which is consistent with previous studies on spin-assisted multilayers (Fig. 2). Also, multilayer thickness strongly depends on polymer molecular weight. The total thicknesses in the H-bonded films consistently rise from 40 to 52, and 60 nm with increasing in PVPON M_w from 2.5 kDa to 55 kDa and 360 kDa (Table 1 and Fig. 2 and 3). The effect of PVPON molecular weight on film growth becomes less pronounced for PVPON-1300. The bilayer thicknesses were found to be 2.4±0.5, 3.3±0.5, 4.3±0.5, and 4.4±0.5 nm for $(PMAA/PVPON\text{-}2.5)_{12}$, $(PMAA/PVPON\text{-}55)_{12}$, $(PMAA/PVPON\text{-}360)_{12}$, and $(PMAA/PVPON\text{-}1300)_{12}$, respectively. The corresponding individual layer thicknesses increase with PVPON M_w for both film constituents and were measured to be 1.1±0.6 nm and 1.7±0.4 nm; 1.0±0.3nm and 2.6±0.4 nm; 1.2±0.4 nm and 3.2±0.5 nm; and 1.4±0.5 nm and 3.1±0.5 nm for PVPON and PMAA, respectively, yielding twice the incremental thickness for each PMAA layer. Based on these data, PVPON-2.5 comprises 39% by film thickness which is smaller compared to the higher M_w polymers, for which the thickness percentage falls in the range from 28% to 31%. These results are consistent with previous studies that reported thicker H-bonded and ionically-paired multilayers

were made with longer polymer chains.[61,62,63] Typically, longer polymers offer more available sites for interactions in their loops and tails,[67] and thus, thicker films. In most cases, this effect is observed up to a certain threshold value in polymer length with the shorter polymer chains affecting film growth more strongly. [68,69] For instance, a significant increase in dipped poly(acrylic acid) (PAA/PEO) multilayer thickness was observed when the PEO molecular weight increased from 1.5 kDa to 20 kDa but only a small further thickness increase was found with PEO of 4000 kDa.[62] Similarly, our recent study showed that silk/poly(N-vinylcaprolactam) (PVCL) films made of 40 kDa PVCL were much thicker than those containing 5 kDa PVCL, but there was no further film thickness increase with 80 kDa PVCL.[69]

In our case, film thickness is strongly influenced by PVPON molecular weight for $M_w \leq 360$ kDa and becomes fairly constant for larger M_w. Except for PVPON-1300, the increase in multilayer thickness alongside molecular weight is consistent with the increase in the PVPON radius of gyration in solutions, R_g. Assuming a PVPON persistence length of 1 nm,[70] the R_g values for PVPON chains are estimated to be 1.0 nm, 4.5 nm, 11.6 nm and 22.1 nm for PVPON-2.5, PVPON-55, and PVPON-360, and PVPON-1300 respectively, giving the corresponding diameters of gyration ($2R_g$) of 2.0 nm, 9.0 nm, 23.2 nm, and 22.1 nm. Interestingly, these values exceed the bilayer thickness starting from PVPON-55 and this effect progresses with increasing polymer M_w. The bilayer thickness is less than $2R_g$ by factors of 3, 6, and 12 for (PMAA/PVPON-55), (PMAA/PVPON-360), and $(PMAA/PVPON\text{-}1300)_{12}$, respectively (Table 1). However, for the shortest PVPON, the $2R_g$ of 2 nm is slightly smaller than the (PMAA/PVPON-2.5) bilayer thickness, 2.4±0.5 nm. These results indicate that PVPON at larger molecular weights is adsorbed in stretched and flattened conformations, without much interdiffusion into the neighboring layers, which is typical for polymers deposited by spinning.[39,40,72] As a result, the bilayer thicknesses for

those systems are much smaller than the diameters of PVPON coils in solutions. In contrast, short-chain PVPON intermixed with the polymer matrix more vigorously, yielding a bilayer thickness slightly larger than the polymer coil diameter. Similarly, decreasing polyanion molecular weight in dipped polyelectrolyte multilayers increases diffusion constants and bilayer thicknesses.[58,60,68] Thus, our data show that the thickness of spin-assisted multilayers can be sensitive to polymer M_w unlike prior studies which showed dipped films to be stronger affected by polymer chain lengths as compared to their spin-assisted counterparts.[59,69]

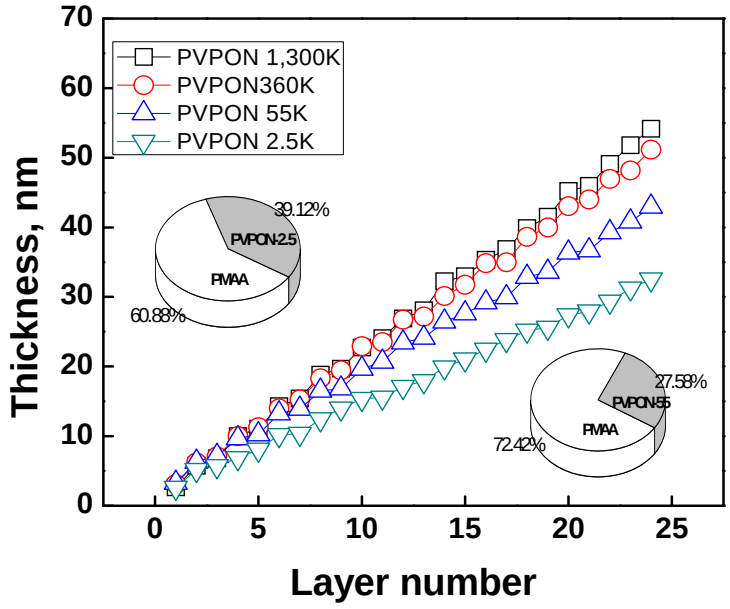

Figure 2. LbL growth of $(PMAA/PVPON\text{-}2.5)_{12}$, $(PMAA/PVPON\text{-}55)_{12}$, $(PMAA/PVPON\text{-}360)_{12}$, and $(PMAA/PVPON\text{-}1300)_{12}$ films at pH=3. Inset shows mass distribution for PMAA and PVPON in $(PMAA\text{-}PVPON\text{-}2.5)_{12}$ and $(PMAA\text{-}PVPON\text{-}55)_{12}$ films. The thickness ratios for $(PMAA/PVPON\text{-}2.5)_{12}$ and $(PMAA/PVPON\text{-}55)_{12}$ films are calculated using an average incremental increase of each polymer layer (given 1 mg m^{-2} adsorbed amount of polymer per 1 nm film thickness).

Internal structure of H-bonded (PMAA/PVPON) films

To study the effect of PVPON molecular weight on multilayer organization, conventional PMAA ($C_4{}^1H_6O_2$) was replaced by its deuterated counterpart *d*PMAA ($C_4{}^2H_6O_2$) in every fifth bilayer during deposition. The dramatically different neutron scattering properties of the proton and the deuteron provided refractive-index contrast and allowed tracking the evolution of PMAA layer structure using neutron specular reflectivity (NR) before and after multilayer crosslinking. NR profiles for as-cast $[(PMAA/PVPON)_4 dPMAA/PVPON]_3(PMAA/PVPON)_2$ films constructed with PVPON of various molecular weights are shown in Figure 3 (left panels). Neutron reflectivity R is plotted *vs* wavevector transfer Q ($Q= 4\pi \sin\theta /\lambda$, where θ is the incident angle and λ is the neutron wavelength). Remarkably, all of our H-bonded films demonstrate well-defined Bragg peaks indicative of a high degree of stratification. The data were fitted using the model described in the Experimental section where initial individual layer thicknesses were taken from ellipsometry data and then adjusted to fit the NR profiles. The corresponding fitted scattering-length-density (SLD) profiles reveal sharply contrasting and well-separated sequences of labelled *d*PMAA layers following distinct SiO_2 peaks originating from the natural silicon oxide layer at the surface of the Si crystal, (Fig. 3). Film thicknesses and scattering parameters found from neutron reflectivity experiments are summarized in Table 1 and Tables S1-S4 in Supporting Information. The total film thicknesses found from neutron reflectivity were 40.5±0.3, 54.4±0.3, 60.3±0.2, and 61.3±0.2 nm for $(PMAA/PVPON\text{-}2.5)_{17}$, $(PMAA/PVPON\text{-}55)_{17}$, $(PMAA/PVPON\text{-}360)_{17}$, and $(PMAA/PVPON\text{-}1300)_{17}$, respectively, which correlates well (±5%) with those measured with ellipsometry. Importantly, in all four systems the *d*PMAA layers are equally spaced with the distance between these layers increasing with the increase in total film thickness, which in turn correlates with the increase in PVPON molecular weight. Another important observation is that

individual marker layers in the $(PMAA/PVPON\text{-}2.5)_{17}$ film are thicker than those in multilayers of larger M_w PVPON. As seen from the SLD profiles, the thicknesses (d_d) of the *d*PMAA layers are 3.5, 2.8, 2.8, and 3.0 nm for 2.5 kDa, 55 kDa, 360 kDa, and 1300 kDa PVPON, respectively. Thus, in the films prepared with 2.5 kDa PVPON, the *d*PMAA is distributed more widely compared to the other systems. This result is in excellent agreement with our ellipsometry data above that showed $d_{bl} > 2R_g$ due to the the strong intermixing of PVPON-2.5 with adjacent layers.

Internal structure of (PMAA) hydrogel films

To produce PMAA networks, all H-bonded films were treated with EDA, followed by exposure of these films to pH = 8 for 24 hours.[30] During this procedure, PVPON of 2.5 kDa, 55 kDa, and 360 kDa was completely released from the crosslinked films, due to disruption of hydrogen bonds between PVPON and ionized PMAA (pK_a~*5.5*). As a result, the thicknesses of the crosslinked films decreased by 30-35% relative to their initial thicknesses, as measured with ellipsometry, which is consistent with previous reports on multilayer-derived PMAA hydrogels.[30,40] These data also correlate well with those on PMAA and PVPON uptake during deposition that imply that about two third of the film is PMAA (Fig.1). However, crosslinking of (PMAA/PVPON-1300) resulted in only an 18% release of PVPON, indicating that the polymer is partially retained in the film. The hindered release of PVPON-1300 can be explained by kinetically trapped chains that require much more time to diffuse out as compared to the shorter PVPON chains. Indeed, increasing polymer molecular weight enhances the degree of chain entanglements and interdiffusion in multilayers. Strongly entangled chains need more time for rearrangement in response to pH-triggered imbalances. Similar effects were observed previously with ionically paired and H-bonded multilayers, which exhibited a slow pH-triggered disintegration when composed of higher M_w polymers.[56,59,68]

Figure 4 compares neutron reflectivity data and the corresponding fitted SLD profiles for all four PVPON molecular weights. The data show that the post-crosslinked films are about 2/3 of the thickness of the as-grown, except the film with PVPON-1300, which is in excellent agreement with our ellipsometry data. A striking feature is the presence of distinct and periodic *d*PMAA layers in the post-crosslinked SLD profiles. This result shows that layering persists after crosslinking, which is indicative of well-defined structure within these hydrogels. At the same time, the crosslinking of all four types of H-bonded systems results in layer interpenetration revealed by peak broadening, a decrease in peak amplitudes, and an increase in internal roughness. The SLDs of the *d*PMAA layers decreased from 3.3×10^{-4} nm^{-2} to 2.5×10^{-4} nm^{-2} before and after crosslinking, respectively, indicating partial intermixing of *d*PMAA with hydrogenated material.

Equally important, the thickness of *d*PMAA layers increases with the PVPON M_w used for film fabrication, inducing increased layer interpenetration upon crosslinking. Similarly, the internal roughness in the hydrogels gradually increases from 2.8 to 4.5 nm with increase in PVPON M_w from 2.5 kDa to 1300 kDa (Table 1 and Tables S5-S8 in Supporting Information). These values are slightly higher than those for the corresponding H-bonded films, progressing from 2.6 to 3.0 nm for PVPON of 2.5 kDa and 1300 kDa, respectively (Table 1), which reveals the extent of mixing upon crosslinking. Remarkably, despite the partial interlayer diffusion, the three marker layers in all four systems are well separated without any change in amplitude with distance from the substrate, revealing that a significant degree of stratification is preserved during the crosslinking process.

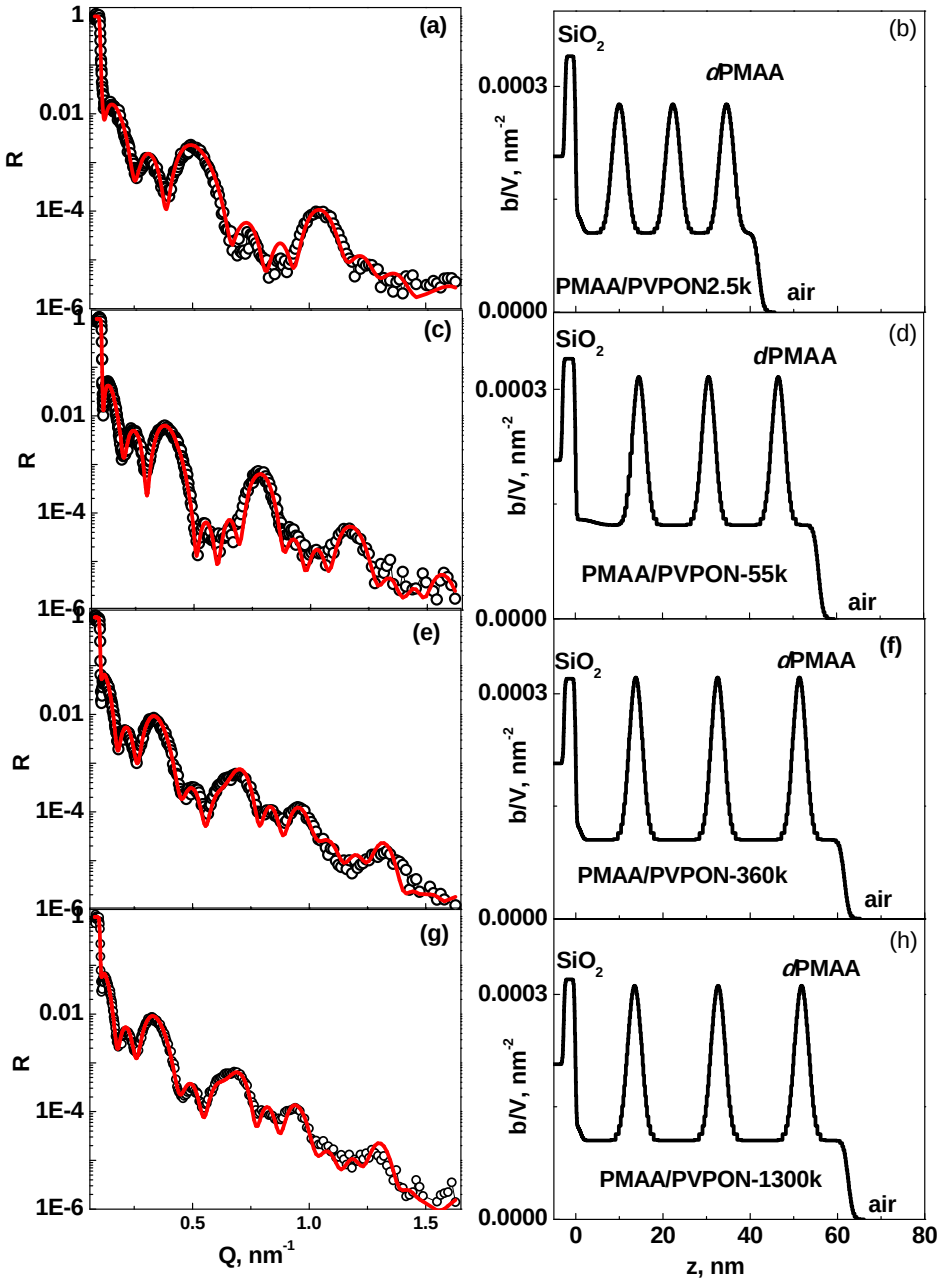

Figure 3. NR data (left panels) and corresponding SLD profiles (right panels) for $[(PMAA/PVPON)_4 d PMAA/PVPON]_3(PMAA/PVPON)_2$ films containing PVPON-2.5 (a,b), PVPON-55 (c,d), PVPON-360 (e,f), and PVPON-1300 (g,h). Open symbols and solid lines show experimental NR data and fit, respectively.

Table 1. Summary of neutron reflectivity, ellipsometry, and AFM parameters for H-bonded films.

LbL systems	PVPON M_w	Film thickness, nm[#]	*d*PMAA thickness, nm	Internal roughness, σ_d, nm	RMS, nm[&]
$(PMAA/PVPON)_{20}$	2.5k	40.6	3.5*	2.6	0.88
$(PMAA/PVPON)_{20}$	55k	51.5	2.8*	2.8	1.08
$(PMAA/PVPON)_{20}$	360k	60.4	2.8*	2.8	1.19
$(PMAA/PVPON)_{20}$	1300k	61.3	3.0*	3.0	1.31

[#] Ellipsometry thickness corresponds to that found with neutron reflectivity within 3% for spin-assisted films; and within 15% for dipped films due to the rough film morphology, * *d*PMAA is deposited as every 5th PMAA layer, [&] RMS found with AFM

Table 2. Summary of ellipsometry, neutron reflectivity, and AFM parameters for hydrogels obtained from films shown in Table 1.

LbL systems	PVPON M_w, kDa	Film thickness, nm	*d*PMAA thickness, nm	Internal roughness, σ_d, nm	RMS
$(PMAA)_{20}$	2.5	31.2	3.8	2.8	1.65
$(PMAA)_{20}$	55	38.3	4.0	4.0	1.08
$(PMAA)_{20}$	360	47.1	4.4	4.4	1.25

$(PMAA)_{20}$	1300	49.4	4.5	4.5	1.17

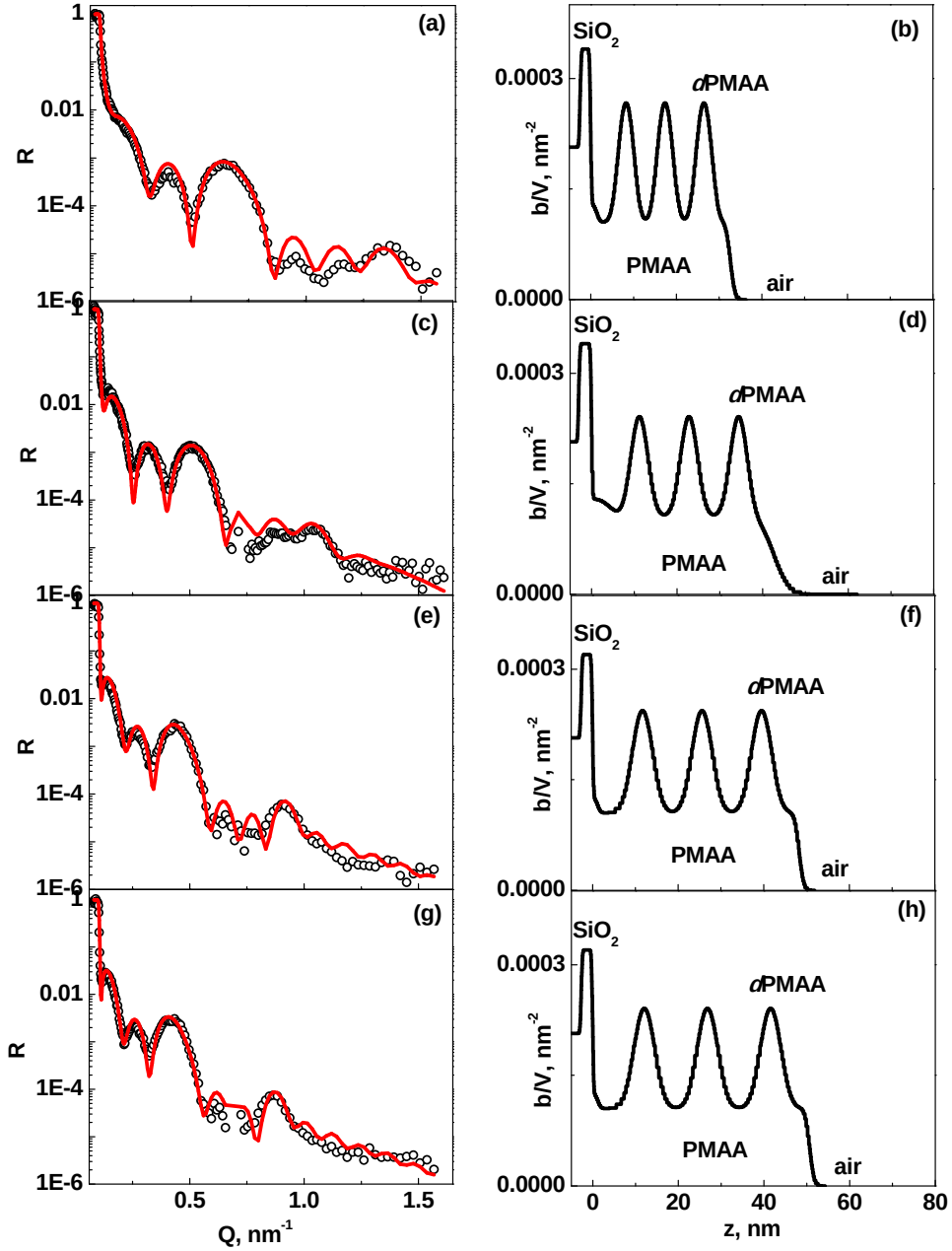

Figure 4. NR data (left panels) and corresponding SLD profiles (right panels) for $[(PMAA)_4dPMAA]_3(PMAA)_2$ films obtained by crosslinking H-bonded films containing PVPON-2.5 (a,b), PVPON-55 (c,d), PVPON-360 (e,f), and PVPON-1300 (g,h). Open symbols and solid lines show experimental NR data and fit, respectively.

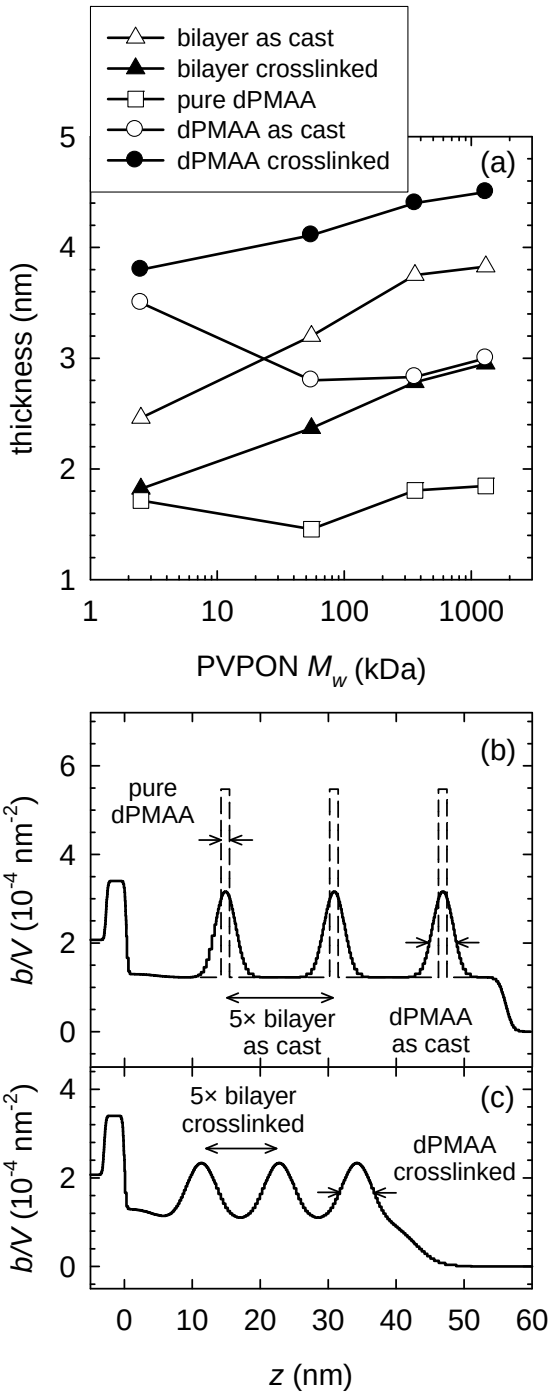

Figure 5. (a) Structural parameters of H-bonded films and corresponding hydrogels made with different M_w PVPON. The model structural features are identified for the same film (M_w = 55 kDa) as cast (b) and crosslinked (c). See the text for a detailed explanation.

Figure 5a compiles the structural data derived from highly constrained neutron specular reflectivity model fits depicted for as-cast (Fig. 5b - the 55 kDa PVPON model from Fig. 3d) and crosslinked films (Fig. 5c - 55 kDa model from Fig. 4d). 'Pure *d*PMAA', *d*PMAA, and bilayer thicknesses are plotted as a function of PVPON molecular weight. The 'pure *d*PMAA' value (open squares) represents a thickness of *d*PMAA 'unmixed' with H-PMAA and accounts for the total amount of *d*PMAA in the films, which is preserved in the crosslinked films. This value was estimated as the ellipsometry increase in film thickness per PMAA deposition step and was further optimized in the neutron reflectivity model (Fig. 5a). In this case, preservation of deposited *d*PMAA over the lifetime of the sample (mass balance) was the key to the data analysis (see experimental section for the details). Likewise from ellipsometry and also from the Q values of the neutron reflectivity superlattice peaks, the distance between *d*PMAA marker layers was found, which is five times the bilayer spacing, depicted as 'bilayer as cast' (open triangles) and 'bilayer crosslinked' (closed triangles) in Fig. 5a. Due to the random-coil structure of the polymer in solution and the intrinsic disorder of the H-binding process during deposition, *d*PMAA is deposited not as a pure thin layer ($b/V = 5.47\times10^{-4}$ nm^{-2}), but instead mixes with and is diluted by protonated material in adjacent layers. While fitting the neutron reflectivity data, we preserve the amount of *d*PMAA by coupling the width of the *d*PMAA marker layer to the difference in scattering density (b/V) between the marker layer and the protonated matrix.[52] The quantity, thickness of 'pure *d*PMAA' × $[(b/V)_{\mathrm{dPMAA}} - (b/V)_{\mathrm{matrix}}]$, is held invariant. In Fig. 5b, the area of the dashed rectangle is the same as that of the peaked curve ('*d*PMAA as cast', open circles in Fig. 5a) it sits atop; likewise the area under the peaks is preserved between Figs. 5b and 5c ('*d*PMAA crosslinked', closed circles in Fig. 5a). The five quantities tracked in Fig. 5a are thus derived from co-refined neutron reflectivity models for samples composed of four different PVPON molecular weights.

As seen from Figure 5a, the bilayer thickness in H-bonded films increases linearly with PVPON M_w, from 2.5 to 3.8 nm with only a slight increase to 3.0 nm for the 1300 kDa matrix (open triangles). The post-crosslinked 'bilayer' thickness (filled triangles) follows the same trend and increases uniformly with M_w. Note that this thickness is lower than that before crosslinking due to the complete loss of PVPON from the films, except for 1300 kDa PVPON which released only partially as was discussed above.

Importantly, all four H-bonded films show well organized layering, the intrinsic property typical for spin-assisted multilayers.[40,53,57,71] Spin-assisted deposition typically results in chain flattening and surface smoothening due to the fast removal of water and loosely bound chains by centrifugal forces, unlike more interdiffused and loopy chains in dipped films.[72,73,74] Figure 5b clearly shows the equally spaced *d*PMAA layers in SLD profiles of a (PMAA/PVPON-55) film. The marker layers are broader and twice lower in scattering density than those for 'pure *d*PMAA' due to partial mixing with hydrogenated polymers. The layering persists after crosslinking (Fig. 5c). However, *d*PMAA is more widely dispersed than in the base H-bonded films due to enhanced chain movement and rearrangements during crosslinking and PVPON release. Interestingly, the distribution of material inside the film expressed through the thickness of the marker layers is controlled by PVPON M_w and differs before and after crosslinking. In H-bonded films, the thickness of *d*PMAA (Fig. 5a, open circles) varies strongly and non-monotonically with PVPON M_w. This thickness decreases sharply from 3.5 to 2.8 nm for the 2.5 kDa and 55 kDa PVPON, respectively, and then remains fairly constant for 360 kDa and 1300 kDa PVPON. This data reveals strong diffusion of the shortest polymer as compared to the longer chains. PMAA deposited with 2.5 kDa PVPON is distributed more widely than a bilayer (3.5 nm), revealing the high mobility of the matrix onto which it binds. In contrast, the thickness of the *d*PMAA after

crosslinking grows monotonically with the PVPON M_w used for film fabrication. Remarkably, these thicknesses are larger than those before crosslinking increasing only slightly for PVPON-2.5 (from 3.5 to 3.7 nm) and more dramatically by a factor of 1.7 for the higher molecular weights (from 2.8 to 4 nm for PVPON-55 and from 2.9 to 4.3 nm for PVPON-360). These results demonstrate a significant degree of layer intermixing and *d*PMAA spreading in the films templated with longer PVPON chains. Note that the thickness of 'pure *d*PMAA' deposited per step (Fig. 5a, open squares) remains fairly constant with PVPON M_w.

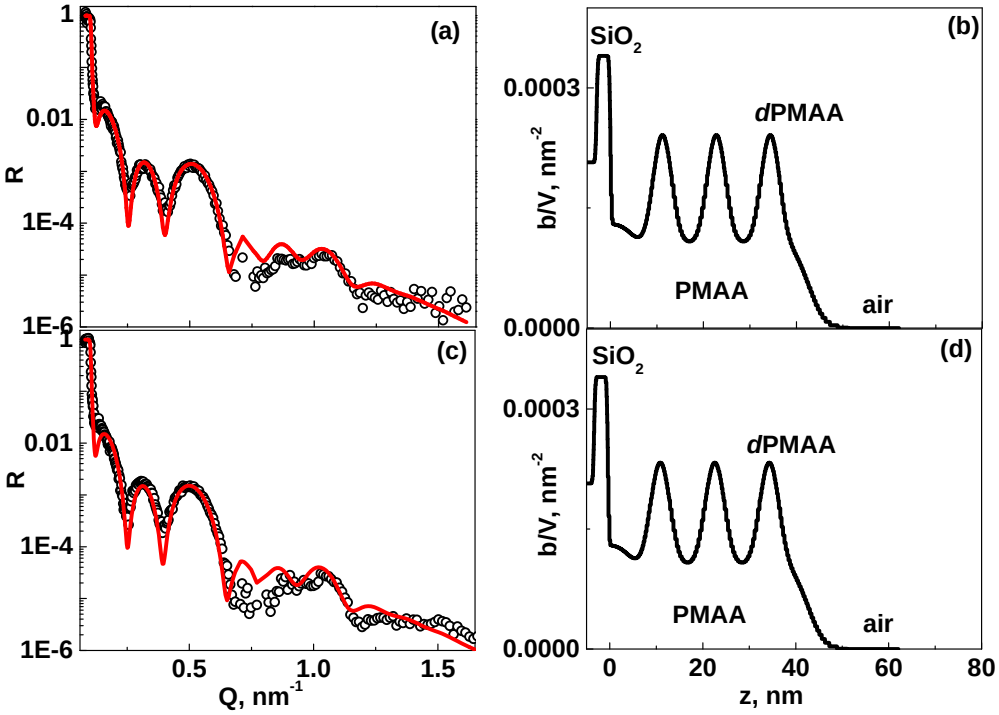

Figure 6. NR data (left panels) and corresponding SLD profiles (right panels) for [(PMAA/PVPON)$_4$*d*PMAA/PVPON]$_3$(PMAA/PVPON)$_2$ films containing PVPON-55 after crosslinking (a,b) and after hydration followed by drying (c,d). Open symbols and solid lines show experimental NR data and fit, respectively.

To test structural stability upon dehydration, PMAA hydrogels, after being measured in dry state, were hydrated by exposure to pH = 8 buffer for 14 hours, followed by drying. The data after crosslinking and dehydration of (PMAA/PVPON-55) are shown in Figure 6 and Table S9 in Supporting information. Notably, well-structured layering persists in the hydrogels upon subsequent dehydration and drying (Fig. 6).

Surface morphology

Finally, AFM was used to explore the surface morphology of $(PMAA/PVPON)_{12}$ films before and after crosslinking films. The AFM topographical images represent surface micro-roughness (root-mean-square roughness) for all four H-bonded films before and after crosslinking and are shown in Figure 7 and 8, respectively. We found that increasing PVPON M_w from 2.5 kDa to 1300 kDa increases surface micro-roughness (RMS) for as-cast films from 0.88±0.2 to 1.3±0.3 nm, respectively, as measured from (1 x 1) μm^2 surface areas (Fig. 7). In contrast, the corresponding PMAA hydrogels are much smoother and show small-grain morphology, a common feature of crosslinked networks[75] (Fig. 8). Another observation is that the RMS values after crosslinking decreased with increase in PVPON M_w, unlike those in the H-bonded films that showed the opposite trend. The RMS roughness of the hydrogels consistently decreased from 1.65±0.2 to 1.17±0.2 nm after crosslinking of (PMAA/PVPON-2.5) and (PMAA/PVPON-1300), respectively (Fig. 8).

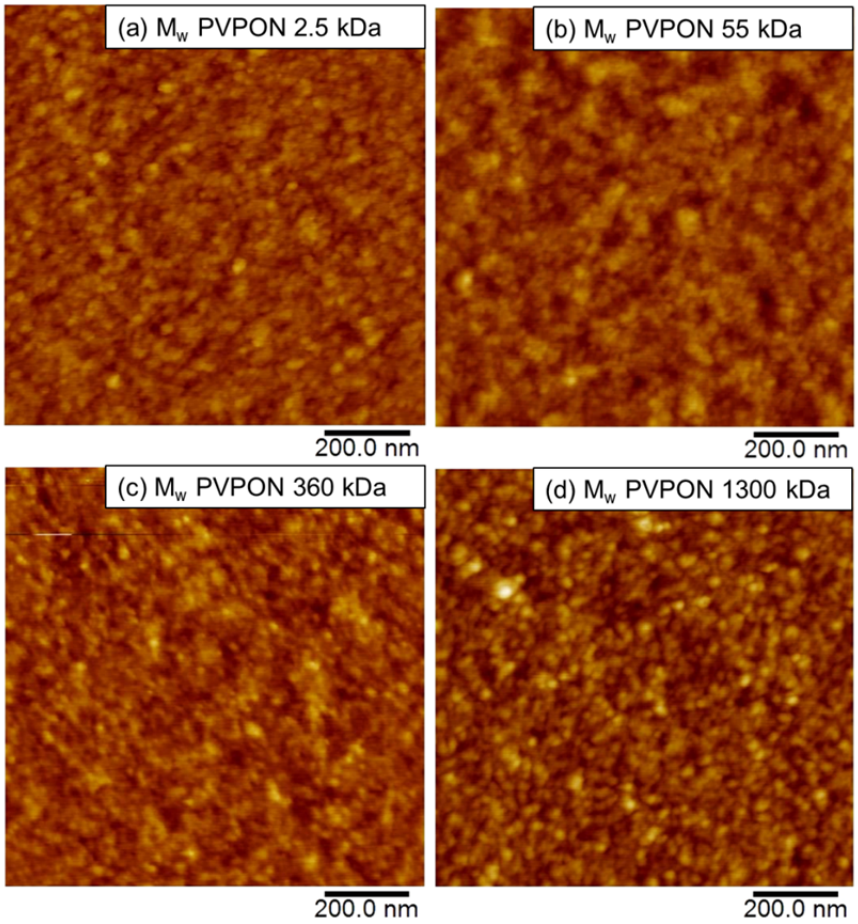

Figure 7. AFM topography images for $(PMAA/PVPON)_{12}$ films containing PVPON-2.5 (a), PVPON-55 (b), PVPON-360 (b), and PVPON-1300 (d). Z-scale is 20 nm. Scale bar is 200 nm.

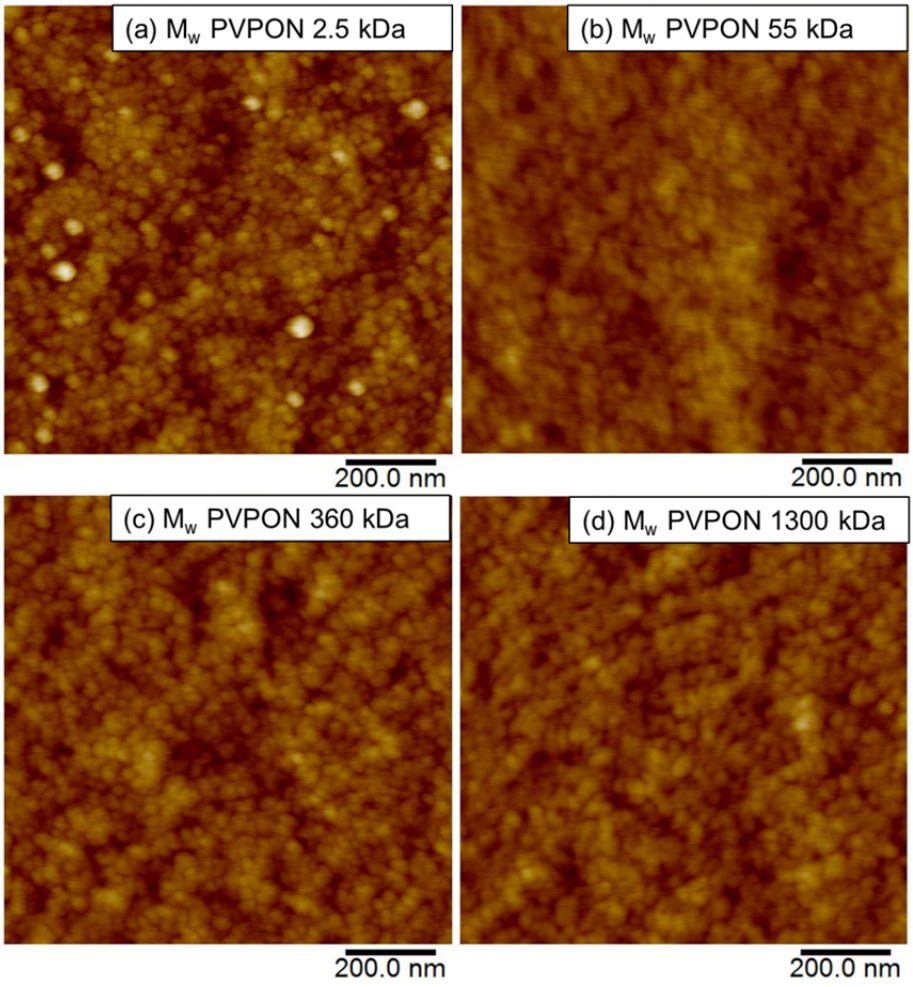

Figure 8. AFM topography images for $(PMAA)_{12}$ hydrogels after crosslinking of $(PMAA/PVPON)_{12}$ films containing PVPON-2.5 (a), PVPON-55 (b), PVPON-360 (b), and PVPON-1300 (d). Z-scale is 20 nm. Scale bar is 200 nm.

General discussion

Our overall data show that PVPON M_w regulates thickness, surface microstructure, and internal organization of both H-bonded films and the corresponding hydrogels with a nanoscale precision. In this respect, the main structural and compositional parameters for the hydrogels are dictated by those for the H-bonded multilayers. As shown above, the total and bilayer thicknesses in both H-bonded precursors and the corresponding PVPON-free hydrogels consistently increase with PVPON M_w from 2.5 to 360 kDa; except PVPON-1300 that partially retained in the networks. Intriguingly, the organization of interior structure in these films, expressed through the internal roughness and thickness of *d*PMAA marker layers, is strongly controlled by PVPON chain length.

First, rise in thickness of H-bonded films with PVPON M_w is consistent with increase in both internal and surface roughness (Table 1). A moderate increase in internal roughness but a more dramatic change in RMS microroughness point to a stronger chain intermixing within the film as compared to that on the surface. Similar results were observed previously that reported rougher surfaces for multilayers cast of higher M_w polymers due to their loopy conformations and higher degree of chain entanglements.[68] In contrast, the crosslinked hydrogels show a decrease is surface roughness with the increase in PVPON M_w. The smoothened morphology with the increase in PVPON chain length indicates enhanced chain flattening. A high surface roughness as a result of short PVPON release correlates well with its high relative proportion in a bilayer as compared to longer PVPON, an indicative of loopy PMAA conformations at the film/air interface. Another distinct feature is that the increase in internal roughness and *d*PMAA thickness with PVPON M_w is more dramatic than that for the H-bonded films.

Second, the distribution of *d*PMAA significantly varies before and after crosslinking and is strongly controlled by PVPON M_w. The H-bonded films reveal the same spreading of *d*PMAA for

the three higher PVPON molecular weights, except that for the shortest PVPON that is distributed twice more broadly. This difference most probably arises from the variation in PVPON conformations adapted during assembly. Despite that spin-assisted polymer chains are deposited in a mobility-limited state, the kinetics of chain movement is controlled by the polymer M_w. In this case, short PVPON diffuses faster into the bulk film upon multilayer assembly than that of higher M_w whose mobility is limited by multiple entanglements. This trend is opposite for the crosslinked films. In the crosslinked networks, *d*PMAA is distributed more largely in the films templated with higher M_w PVPON, revealing more pronounced chain interdiffusion. In this case, the quality of network layering is controlled by the kinetics of PVPON release. Most probably, longer PVPON chain stimulate a higher degree of disorder being released from the multilayers since they intertwined more strongly with the adjacent layers and, thus require longer time for rearrangements. In contrast, shorter PVPON releases more rapidly without disturbing layering significantly that correlates well the previous studies that reported on faster release kinetics of low M_w PMAA from ionically paired films.[56]

Finally, despite the variation in mixed interfaces, all three types of PVPON-free hydrogels preserve the initial periodicity of the marker layers. In this case, the well organized structure of the hydrogels develops from the high level of ordering in the as-grown H-bonded templates. The layer stratification persists in all networks including those templated with PVPON of high M_w. The striking feature is that release of PVPON upon crosslinking does not disturb layer ordering. We have recently shown that the architecture of H-bonded dipped films was severely affected by crosslinking, resulting in a highly disordered film with a surface significantly rougher than that before crosslinking.[40] A total loss of internal structure upon release of one of the film components was also observed with dipped electrostatically bound films.[56] In contrast to those systems, in the

hydrogels studied here, the *d*PMAA marker layers remain coherent and can withstand the disorder associated with the driving off of PVPON, despite the fact that spin-assisted chains should be associated more strongly than those in the dipped films. Apparently the kinetics of EDA crosslinking and the following PVPON diffusion are finely enough balanced to preserve the as-cast structure of the films.

Conclusions

We have shown that thickness, surface microstructure, and internal organization of the as-deposited H-bonded (PMAA/PVPON) multilayers and the corresponding (PMAA) multilayer hydrogels are strongly influenced by PVPON M_w. First, thicknesses of both H-bonded films and the hydrogels consistently increase with PVPON M_w from 2.5 to 360 kDa; except PVPON-1300 that partially retained in the networks after crosslinking. Second, increasing polymer M_w smoothens the H-bonded film surfaces but roughens those of the hydrogels. Third, the organization of interior structure, expressed through the internal roughness and thickness of *d*PMAA marker layers, is strongly controlled by PVPON chain length. In the H-bonded films prepared with 2.5 kDa PVPON, *d*PMAA is distributed more widely that that for the larger PVPON molecular weights due to a higher mobility of short PVPON. In addition, the PVPON diameters of gyration in H-bonded films exceed bilayer thickness except for the short-chain PVPON whose $2R_g$<dbl due to the vigorous intermixing with the polymer matrix. In contrast, in the crosslinked networks, *d*PMAA is distributed more largely in the films templated with higher M_w PVPON, revealing more pronounced chain interdiffusion. Finally, despite the variation in mixed interfaces, all three types of hydrogels preserve high degree of stratification found in the as-grown H-bonded templates indicating that release of PVPON upon crosslinking does not disturb layer ordering. Our results are

relevant to both fundamental and applied research where control of the film architecture on a nanometre scale is crucial.

Acknowledgment. This work was supported by NSF Career Award #1350370 (EK) and by EPSCoR DOE/JINS Travel Fellowship. ORNL is managed by UT-Battelle, LLC, for the US Department of Energy (DOE) under contract no. DE-AC05- 00OR22725.

Supporting Information Available: Scattering parameters found from neutron reflectivity experiments for H-bonded and hydrogel films. This material is available free of charge via the Internet at http://pubs.acs.org

References

1. Osada, Y.; Gong, J. P.; Tanaka, Y. *J. Macromol. Sci, C: Polymer Reviews* **2004**, *44*, 87-112.

2. Am Ende, M. T.; Hariharan, D.; Peppas, N. A. *Reactive Polymers* **1995**, *25*, 127-137.

3. Zeng, J.; Tikare, V.; Jacob, K. I. *Langmuir* **2006**, *22*, 1333-1340.

4. Beebe, D. J.; Moore, J. S.; Bauer, J. M.; Yu, Q.; Liu, R. H.; Devadoss, C.; Jo, B.-H. *Nature* **2000**, *404*, 588-590.

5. Zhao, B.; Moore, J. S. *Langmuir* **2001**, *17*, 4758-4763.

6. Tanaka, T.; Fillmore, D. J. *J. Chem. Phys.* **1979**, *70*, 1214-1218.

7. Peppas, N.; Leobandung, W. *J. Biomaterials Science. Polymer Edition* **2004**, *15*, 125-144.

8. Holtz, J. H.; Asher, S. A. *Nature* **1997**, *389*, 829-832.

9. Lee, Y.-J.; Pruzinsky, S. A.; Braun, P. V. *Langmuir* **2004**, *20*, 3096-3106.

10. Leonard, M.; De Boisseson, M. R.; Hubert, P.; Dalençon, F.; Dellacherie, E. *J. Controlled Release* **2004**, *98*, 395-405.

11. Kharlampieva, E.; Erel-Unal, I.; Sukhishvili, S. A. *Langmuir* **2007**, *23*, 175-181.

12. Tokarev, I.; Minko, S. *Adv. Mater*. **2009**, *21*, 241-247.

13. Ladet, S.; David, L.; Domard, A. *Nature* **2008**, *452*, 76-80.

14. Dai, H.; Li, X.; Long, Y.; Wu, J.; Liang, S.; Zhang, X.; Zhao, N.; Xu, J. *Soft Matter* **2009**, *5*, 1987-1989.

15. Johson, L. M.; DeForest, C. A.; Pendurti, A.; Anseth, K. S.; Bowman, C. N. *ACS Appl. Mater. & Interfaces* **2010**, *2*, 1963-1972.

16. Kizilel, S.; Sawardecker, E.; Teymour, F.; Perez-Luna, V. H. *Biomaterials* **2006**, *27*, 1209-1215.

17. Mjahed, H.; Porcel, C.; Senger, B.; Chassepot, A.; Netter, P.; Gillet, P.; Decher, G.; Voegel, J-C.; Schaaf, P.; Benkirane-Jessel, N.; Boulmedais, F. *Soft Matter* **2008**, *4*, 1422-1429.

18. Appel, E. A.; Loh, X. J.; Jones, S. T.; Biedermann, F.; Dreiss, C. A.;. Scherman, O. A. *J. Am. Chem. Soc*. **2012**, *134*, 11767-11773.

19. Lee, W.; Son, J.; Yoo, S. -S.; Park, J. -K. *Biomacromolecules* **2011**, *12*, 14-28.

20. Engel, B. J.; Constantinou, P. E.; Sablatura, L. K.; Doty, N. J.; Carson, D. D.; Farach-Carson, M. C.; Harrington, D. A.; Zarembinski, T. I. *Adv. Healthcare Mater*. **2015**, *4*, 1664-1674.

21 Asoh, T.-A.; Kawamura, E.; Kikuchi, A. *RSC Adv*. **2013**, *3*, 7947-7952.

22. Kozlovskaya, V.; Kharlampieva, E.; Erel-Unal, I.; Sukhishvili, S. A. *Soft Matter* **2009**, *5*, 4077-4087.

23. Yang, S. Y.; Rubner, M. F. *J. Am. Chem. Soc*. **2002**, *124*, 2100-2101 .

24. Johnston, A. P. R.; Cortez, C.; Angelatos, A. S.; Caruso, F. *Curr. Opin. Colloid Interface Sci*. **2006**, *11*, 203-209.

25. Hammond, P. T. *Adv. Mater*. **2004**, *16*, 1271-1293.

26. Tokarev, I.; Minko, S. *Adv. Mater*. **2010**, *22*, 3446-3462.

27. Guzmán, E.; Ritacco, H.; Rubio, J. E. F.; Rubio, R. G.; Ortega, F. *Soft Matter* **2009**, *5*, 2130-2142.

28. Guzmán, E.; Ritacco, H. A.; Ortega, F.; Rubio, R. G. *J. Phys. Chem. C* **2012**, *116*, 15474-15483.

29. Lee, D.; Cohen, R. E.; Rubner, M. F. *Langmuir* **2005**, *21*, 9651-9659.

30. Kozlovskaya, V.; Wang, Y.; Higgins, W.; Chen, J.; Chen, Y.; Kharlampieva, E. *Soft Matter* **2012**, *8*, 9828- 9839.

31. Kozlovskaya, V.; Alexander, J.; Wang, Y.; Kuncewicz, T.; Liu, X.; Godin, B.; Kharlampieva, E. *ACS Nano* **2014**, *8*, 5725-5737.

32. Shimoni, O.; Yan, Y.; Wang, Y.; Caruso, F. *ACS Nano* **2013**, *7*, 522-530.

33. Duan, J.; Hou, R.; Xiong, X.; Wang, Y.; Wang, Y.; Fu, J.; Yu, Z. *J. Mater. Chem. B* **2013**, *1*, 485-492.

34. Serizawa, T.; Matsukuma, D.; Nanameki, K.; Uemura, M.; Kurusu F.; Akashi, M. *Macromolecules* **2004**, *37*, 6531-6536.

35. Bergbrieter, D. E.; Chance, B. S. *Macromolecules* **2007**, *40*, 5337-5343.

36. Rydzek, G.; Schaaf, P.; Voegel, J.-C.; Jierry, L.; Boulmedais, F. *Soft Matter* **2012**, *8*, 9738-9755.

37. Wang, H.; Zha, G.; Du, H.; Gao, L.; Li, X.; Shen, Z.; Zhu, W. *Polym. Chem*. **2014**, *5*, 6489-6494.

38. Kozlovskaya, V.; Higgins, W.; Chen, J.; Kharlampieva, E. *Chem. Commun*. **2011**, *47*, 8352-8354.

39. Wang, Y.; Kozlovskaya, V.; Arcibal, I.; Cropek, D.; Kharlampieva, E. *Soft Matter* **2013**, *9*, 9420-9429.

40. Kozlovskaya, V.; Zavgorodnya, O.; Wang, Y.; Ankner, J. F.; Kharlampieva, E. *ACS Macro Lett.* **2013**, 2, 226-229.

41. Zavgorodnya, O.; Kozlovskaya, V.; Liang, X.; Kothalawala, N.; Catledge, S.; Dass, A.; Kharlampieva, E. *Mater. Res. Express* **2014**, *1*, 035039.

42. Lavalle, P.; Voegel, J.-C.; Vautier, D.; Senger, B.; Schaaf, P.; Ball, V. *Adv. Mater*. **2011**, *23*, 1191-1221.

43. Pavlukhina, S.; Lu, Y.; Patimetha, A.; Libera, M.; Sukhishvili, S. *Biomacromolecules* **2010**, *11*, 3448-3456.

44. Schmitt, J.; Grünewald, T.; Decher, G.; Pershan, P. S.; Kjaer, K.; Lösche, M. *Macromolecules* **1993**, *26*, 7058-7063.

45. Kellogg, G. J.; Mayes, A. M.; Stockton, W. B.; Ferreira, M.; Rubner, M. F.; Satija, S. K. *Langmuir* **1996**, *12*, 5109-5113.

46. Von Klitzing, R. *Phys. Chem. Chem. Phys*. **2006**, *8*, 5012-5033.

47. Jablin, M. S.; Dubey, M.; Zhernenkov, M.; Toomey, R.; Majewski, J. *Biophys. J.* **2011**, *101*, 128-133.

48. Jean, B.; Heux, L.; Dubreuil, F.; Chambat, G. Cousin, F. *Langmuir* **2009**, *25*, 3920-3923.

49. Gopinadhan, M.; Ivanova, O.; Ahrens, H.; Günther, J. -U. Steitz, R.; Helm, C. A. *J. Phys. Chem. B* **2007**, *111*, 8426-8434.

50. Singh, S.; Junghans, A.; Watkins, E.; Kapoor, Y.; Toomey, R.; Majewski, J. *Langmuir* **2015**, *31*, 2870-2878.

51. Guzmán, E.; Ritacco, H.; Ortega, F.; Rubio, R. G. *Colloids Surf., A* **2011**, *384*, 274-281

52. Kharlampieva, E.; Kozlovskaya, V.; Ankner, J. F.; Sukhishvili, S. A. *Langmiur* **2008**, *24*, 11346-11349.

53. Kozlovskaya, V.; Ankner, J. F.; O'Neill, H.; Zhang, Q.; Kharlampieva, E. *Soft Matter* **2011**, *7*, 11453-11463.

54. Lösche, M.; Schmitt, J.; Decher, G.; Bouwman, W. G.; Kjaer, K. *Macromolecules* **1998**, *31*, 8893-8906.

55. Jomaa, H. W.; Schlenoff, J. B. *Macromolecules* **2005**, *38*, 8473-8480.

56. Kharlampieva, E.; Ankner, J. F.; Rubinstein, M. Sukhishvili, S. A. *Phys.Rev. Lett.* **2008**, *100*, 128303/1-128303/4.

57. Kharlampieva, E.; Kozlovskaya, V.; Chan, J.; Ankner, J. F.; Tsukruk, V. V. *Langmuir* **2009**, *25*, 14017-14024.

58 Xu, L.; Selin, V.; Zhuk, A.; Ankner, J. F.; Sukhishvili, S. A. *ACS Macro Lett*. **2013**, *2*, 865-868.

59. Jang. Y.; Seo, J.; Akgun, B.; Satija, S.; Char, K. *Macromolecules* **2013**, *46*, 4580-4588.

60. Selin, V.; Ankner, J. F.; Sukhishvili, S. A. *Macromolecules* **2015**, *48*, 3983-3990.

61. Stockton, W. B.; Rubner, M. F. *Macromolecules* **1997**, *30*, 2717-2725.

62. DeLongchamp, D.; Hammond, P. T. *Langmuir* **2004**, *20*, 5403-5411.

63. Guan, Y.; Yang, S.; Zhang, Y.; Xu, J.; Han, C. C.; Kotov, N. A. *J. Phys. Chem. B* **2006**, *110*, 13484-13490.

64. Yang, S.Y.; Lee, D.; Cohen, R. E.; Rubner, M. F. *Langmuir* **2004**, *20*, 5978-5981.

65. Sidorenko, A.; Krupenkin, T.; Aizenberg, J. *J. Mater. Chem*. **2008**, *18*, 3841-3846.

66. Liang, X.; Kozlovskaya, V.; Chen, Y.; Zavgorodnya, O.; Kharlampieva, E. *Chem. Mater*. **2012**, *24*, 3707-3719.

67. Fleer, G.J.; van Male, J.; Johner, A. *Macromolecules* **1999**, *32*, 825-844.

68. Nestler, P.; Paβvogel, M.; Helm, C. A. *Macromolecules* **2013**, *46*, 5622-5629.

69. Espinoza-Dzib, A.; Chen, J.; Zavgorodnya, O.; Kozlovskaya, V.; Liang, X.; Kharlampieva, E. *Soft Matter* **2015**, *11*, 5133-5145.

70. Knappe, P.; Bienert, R.; Weidner, S.; Thuenemann, A. F. *Polymer* **2010**, *51*, 1723-1727.

71. Jang, Y.; Akgun, B.; Kim, H.; Satija, S.; Char, K. *Macromolecules* **2012**, *45*, 3542-3549.

72. Cho, J.; Char, K.; Hong, J.-D.; Lee, K.-B. *Adv. Mater*. **2001**, *13*, 1076-1078.

73. Chiarelli, P. A.; Johal, M. S.; Casson, J. L.; Roberts, J. B.; Robinson, J. M.; Wang, H.-L. *Adv. Mater*. **2001**, *13*, 1167-1171.

74. Lefaux, C. J.; Zimberlin, J. A.; Dobrynin, A. V.; Mather, P. T. *J. Polym. Sci. B: Pol. Phys*. **2004**, *42*, 3654-3666.

75. Kozlovskaya, V.; Kharlampieva, E.; Khanal, B. P.; Manna, P.; Zubarev, E. R.; Tsukruk, V. V. *Chem. Mater*. **2008**, *20*, 7474-7485.